



Airfoil Design for Morphing Wing Using Robust Multiobjective Optimization

メタデータ	言語: eng 出版者: 公開日: 2017-11-21 キーワード (Ja): キーワード (En): 作成者: Kogiso, Nozomu, Toyoda, Masahiro, Funahashi, Takashi, Yokozeki, Tomohiro メールアドレス: 所属:
URL	http://hdl.handle.net/10466/15653

Airfoil Design for Morphing Wing Using Robust Multiobjective Optimization

Nozomu Kogiso^{1*}, Masahiro Toyoda¹, Takashi Funahashi¹ and Tomohiro Yokozeki²

¹ Department of Aerospace Engineering, Osaka Prefecture University, Sakai, Japan.

² Department of Aeronautics and Astronautics, The University of Tokyo, Tokyo, Japan.

Abstract

This study considers the robust optimum airfoil shape of the morphing wing using the corrugated structures arranged in the rear side of the airfoil. The rear side of the wing is deformed like the plain flap by bending the corrugated structure. As the first step, this study considers the multiobjective optimization of the airfoil shape with different objectives corresponding to the flapping angle. In addition, uncertainty of the airfoil shape is considered, thus, the robust multiobjective optimization method is applied. The morphing part is modeled by nonuniform rational basis spline (NURBS) curve and the passing points of the NURBS curve are treated as design variables. In addition, the NURBS curve is smoothly connected by appropriately arranging the passing points to the front side of the airfoil where is not morphed. The aerodynamic analysis is performed by the free computational tool for the wing operating at low Reynolds number range. Then, the surrogate model is constructed using the radial basis function (RBF) network for computationally efficient optimization. Through numerical calculation, the validity of the robust multiobjective optimization method for the airfoil design is demonstrated.

1 INTRODUCTION

A morphing wing can be defined as one which has the ability to either alter its shape in a seamless change along the chord or spar by warping or bending [1, 2]. Yokozeki et al., one of the authors, have developed the variable camber morphing airfoil arranging corrugated structures at the rear side in airfoil as shown in Fig. 1 [3]. Since the corrugated structure has flexibility to bending to the wavy direction, the rear part of the airfoil can morph as a plain flap. The flap has several functions to increase the lift-to-drag ratio at taking off or to increase the lift at approaching. Feasibility of the corrugated morphing airfoil was demonstrated through wind tunnel test using the two-dimensional model [3]. In addition, it is shown that the morphing shape can be designed in terms of the corrugation pitch or the thickness [4]. However, the optimized corrugate arrangement is not studied yet.

Thus, this study applies the robust multiobjective optimum design method proposed by the authors [5] to the airfoil design of the corrugated morphing airfoil. For the formulation of the multiobjective optimization, the satisficing trade-off method (STOM) [6] is applied. STOM is known to be an interactive optimization method and converts a multiobjective optimization problem into the equivalent single-objective optimization problem by introducing an aspiration level that corresponds to the user's preference for each objective function value. In the robust multiobjective optimization, the Pareto solutions are

* kogiso@aero.osakafu-u.ac.jp

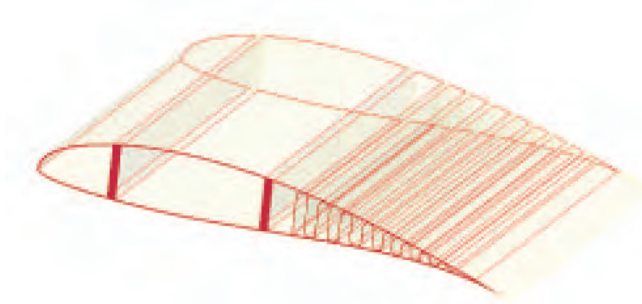


Figure 1. Morphing airfoil using corrugated structure

evaluated to visualize the trade-off between the mean performance and the variation by formulating them as independent objective functions. In previous study, the method was applied to the high high-precision space reflector design to investigate the effect of variations on the applied load on the shape accuracy [7].

As the first step of the optimum design study, this study concentrates on the airfoil shape design considering the aerodynamic performance. The corrugation arrangement design is not considered yet. That will be possible to design the arrangement according to the desired airfoil shape. The morphing wing warped the corrugated section such that the length of the upper curve is unchanged, while that of the lower curve is shrunk [3]. Accordingly, the upper curve is modeled by using the non-uniform rational basis spline (NURBS) curve [8] and the passing points are treated as design variables. The NURBS curve is widely used in the shape optimization such that the airfoil optimization [9] and the membrane design [10]. The curve is modeled under following constraints that the length of the upper curve is unchanged and the morphing part is smoothly connected to the unmorphed front part, where the front part is not modeled as the NURBS curve. In addition, the lower curve of the morphed part is also modeled as the NURBS curve that the passing points are modeled as dependent variables such that the airfoil thickness is unchanged.

The aerodynamic performance is evaluated by using the airfoil analysis tool XFLR5 [11] that is widely adopted to the design of wings operating at low Reynolds numbers. In this study, the numerical analysis tool is not directly used in the optimization. For computational efficiency, the surrogate model [12] is constructed by using the radial basis function (RBF) network [13]. The RBF network constructs the approximation model from several sample points and updates the model by adding the sample properly determined to improve the approximation accuracy. In this study, the RBF network method proposed by Kitayama et al. [14] is adopted for approximation accuracy.

Through numerical examples, it is first demonstrated the efficiency of the morphing airfoil modeling using the NURBS curve proposed in this study. Then, the approximate accuracy of the RBF network for the aerodynamic performance in terms of the design variables, the passing points of the NURBS curve, is discussed. Finally, the usefulness and the efficiency of the robust multiobjective optimization method to the morphing airfoil design are discussed.

2 MORPHING AIRFOIL SHAPE BY NURBS CURVES

The morphing airfoil with corrugation [3] is morphed as the plain flap by bending the corrugation such that the length of the upper curve is unchanged, while that of the lower curve is shrunk as shown in Fig. 2. In addition, the airfoil thickness is unchanged during the morphing.

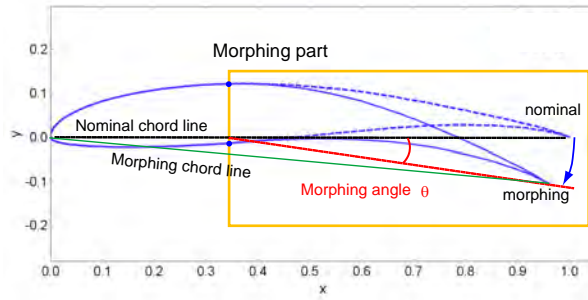


Figure 2. Deformation of morphing wing like plain flap

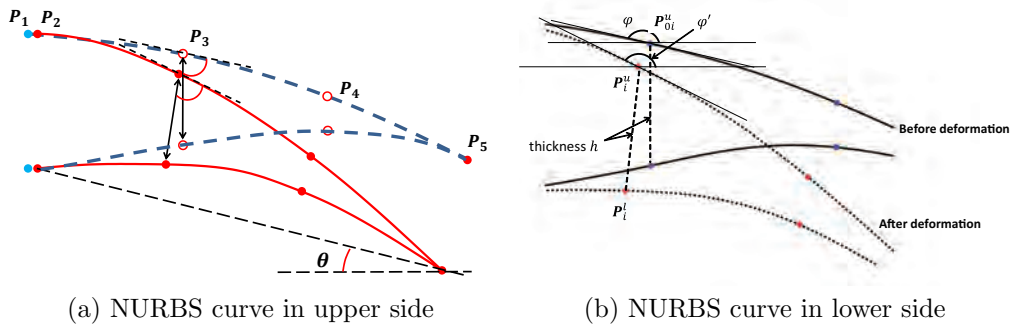


Figure 3. NURBS curve model of morphing part in airfoil

The NURBS curve is adopted to model the morphing section of the rear part of the airfoil. While, the front part without morphing is not modeled as the NURBS curve. Since the total airfoil shape is modeled with a set of nodes passing on the airfoil and the shape is used as an input model to the aerodynamic analysis tool, the nodal points of the rear side are obtained from the NURBS curve and those of the front side are given as the constant values from the airfoil section data. Therefore, the different modeling method for the ordinal airfoil shape optimization using the NURBS curve is required. Especially, the smooth connection is required at the NURBS starting point.

In this study, the NURBS curve passing points are treated as design variables. For efficient optimization, smaller number of the design variables is desirable. The minimum number of the NURBS curve passing points is set to five for sufficient freedom of the airfoil shape and satisfy the smooth connection requirement at the morphing starting point.

At first, consider the upper curve of the airfoil. The NURBS passing point P_2^u is set at the morphing starting point on the upper curve and the another point P_1^u is set at the closed leading edge side on the upper curve as shown in Fig. 3(a), where P_1^u is a starting point of the NURBS curve. The unmoved two points will act such that the change on the curvature of the NURBS curve will be continuous during the morphing for the smooth connection between the front and the rear side. Then, P_5^u is set at the trailing edge point that is the end point of the NURBS curve. The position of the end point P_5^u is determined to satisfy the two conditions as the morphing angle θ and the unchanged length of the upper curve. Where, the morphing angle is defined to the angle between the unmorphed chord line and the line connecting the morphing starting point at the lower curve and the trailing edge as shown in Fig. 2.

The two passing points P_3^u and P_4^u between the starting and the end points on the upper curve are

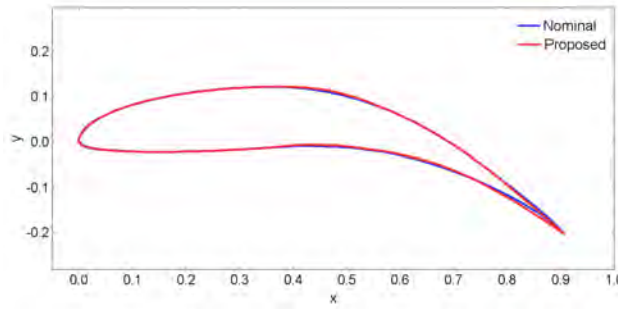


Figure 4. Comparison between NURBS model and original morphing airfoil [3] for 20 degree of morphing angle

freely moved to change the airfoil shape. For sufficient freedom of the airfoil shape and simplicity, the y -coordinates of the points are treated as design variables.

Then, the morphing shape of the lower curve is defined. At first, \mathbf{P}_1^l and \mathbf{P}_2^l are set at the points on the lower curve shifted perpendicular to the unmorphed chord line that is identical to the x -axis. The end points \mathbf{P}_5^l is set as the trailing edge that is identical to \mathbf{P}_5^u as the end point of the upper NURBS curve. Then, the points on the lower curve \mathbf{P}_3^l and \mathbf{P}_4^l are defined as shifting the wing thickness unchanged from the points \mathbf{P}_3^u and \mathbf{P}_4^u on the upper surface, as shown in Fig. 3(b). The wing thickness h_j is first defined for the unmorphed wing as follows:

$$h_j = y_{0j}^u - y_{0j}^l \quad (j = 3, 4) \quad (1)$$

where y_{0j}^u and y_{0j}^l are the y -coordinate of the NURBS passing points for the unmorphed airfoil. As shown in Fig. 3(b), the slope angle of the upper curve at the point is denoted as φ . Then, the passing point coordinate for the morphed airfoil is denoted as $\mathbf{P}^u = [x^u, y^u]$. The coordinate of the corresponding points $\mathbf{P}^l = [x^l, y^l]$ in the lower curve for the morphed wing is evaluated as follows:

$$x^l = x^u - h \sin(\varphi - \varphi') \quad (2)$$

$$y^l = y^u - h \cos(\varphi - \varphi') \quad (3)$$

where φ' is the slope angle at the upper curve for the morphed wing.

Figure 4 compares the morphing airfoil with 20 degree of the morphing angle between the NURBS modeling by red curves and the original shape in reference [3] by blue curves. It is found that the two curves are almost identical, though small differences appear around the trailing edge.

3 AIRFOIL ANALYSIS AND SURROGATE MODEL

3.1 Airfoil analysis

This study uses the airfoil analysis tool XFLR5 [11] that is widely adopted to the design of wings operating at low Reynolds numbers. The tool provides the change of the lift coefficient, the drag coefficient and the moment coefficient with respect to the angle of attack based on the pressure distributions evaluated by the two-dimensional viscous formulation for the given airfoil shape, the velocity, and the Reynolds number.

3.2 Surrogate Model by RBF Network

A radial basis function (RBF) network is a three-layer feed-forward network using the RBF. The function $f(\mathbf{x})$, the output of the network, is approximated as follows:

$$f(\mathbf{x}) = \sum_{j=1}^m w_j h_j(\mathbf{x}) \quad (4)$$

where m indicates the number of sampling points, w_i is the weighting factor, and $h_j(\mathbf{x})$ is the j -th basis function defined as follows:

$$h_j(\mathbf{x}) = \exp \left[-\frac{(\mathbf{x} - \mathbf{x}_j)^T (\mathbf{x} - \mathbf{x}_j)}{r_j^2} \right] \quad (5)$$

where \mathbf{x}_j is j -th sampling point, and r_j is the width of the basis function. In this study, r_j is defined by using Kitayama's method [14] as follows:

$$r_j = \frac{d_{j,\max}}{\sqrt[n]{m-1}} \quad (6)$$

where n is the number of design variables, m denotes the number of sampling points, and $d_{j,\max}$ is the maximum distance between the j -th sample point and the other sampling points.

The RBF network is usually accomplished by solving the following function to estimate the weighting factor \mathbf{w} in Eq. (5).

$$\text{Minimize : } \sum_{i=1}^p (\hat{y}_i - f(\mathbf{x}_i))^2 + \sum_{j=1}^m \lambda_j w_j^2 \quad (7)$$

where the first term is sum of squares of the error between the network output $f(\mathbf{x}_i)$ and the true value \hat{y}_i and the second term is introduced for the regularization [13]. It is recommended that λ_j is set as a small value, e.g., 1×10^{-3} .

The necessary condition of Eq. (7) yields the following equation:

$$\mathbf{w} = (\mathbf{H}^T \mathbf{H} + \boldsymbol{\lambda})^{-1} \mathbf{H}^T \hat{\mathbf{y}} \quad (8)$$

where \mathbf{H} is given as follows:

$$\mathbf{H} = \begin{bmatrix} h_1(\mathbf{x}_1) & h_2(\mathbf{x}_1) & \cdots & h_m(\mathbf{x}_1) \\ h_1(\mathbf{x}_2) & h_2(\mathbf{x}_2) & \cdots & h_m(\mathbf{x}_2) \\ \vdots & \vdots & \ddots & \vdots \\ h_1(\mathbf{x}_p) & h_2(\mathbf{x}_p) & \cdots & h_m(\mathbf{x}_p) \end{bmatrix} \quad (9)$$

and the following matrix \mathbf{A} is introduced:

$$\mathbf{A} = (\mathbf{H}^T \mathbf{H} + \boldsymbol{\lambda}) \quad (10)$$

The learning of the RBF network reduces to obtain \mathbf{A}^{-1} . In this study, the leave one out cross validation (LOOCV) [12] is adopted for efficient learning.

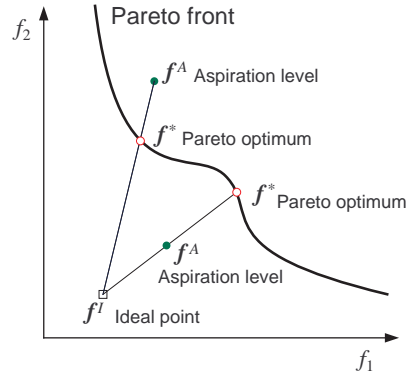


Figure 5. Pareto optimal solution searching by STOM

4 ROBUST MULTIOBJECTIVE OPTIMIZATION

Designing the morphing airfoil requires the robust design that considers the effect of uncertainties of several parameters such as velocity, the angle of attack, the airfoil shape and so on.

The robust optimization can be defined as a multiobjective optimization problem to minimize both the expected value and the variation of the objective function. However, it has been generally formulated as the minimization of the weighted sum of the expected value and the variation as follows:

$$F_{robust}(\mathbf{x}, \mathbf{z}) = E[f(\mathbf{x}, \mathbf{z})] + \alpha \sqrt{\text{Var}[f(\mathbf{x}, \mathbf{z})]} \quad (11)$$

where \mathbf{x} and \mathbf{z} denotes design variables and random variables, respectively, and $\alpha > 0$ is a weight coefficient. The single-objective optimization using Eq. (11) sometimes fails to obtain the desired solution, especially when the Pareto set has a non-convex shape.

In this study, the robust design optimization is formulated as the following multiobjective optimization problem:

$$\text{Minimize: } f_1(\mathbf{x}, \mathbf{z}) = E[f(\mathbf{x}, \mathbf{z})] \quad (12)$$

$$f_2(\mathbf{x}, \mathbf{z}) = \sqrt{\text{Var}[f(\mathbf{x}, \mathbf{z})]} \quad (13)$$

where the expected value and the standard deviation are adopted as individual objective functions.

Part of the authors [5] are proposed to use STOM [6] to the robust multiobjective optimization problems. STOM is known to be an interactive optimization method and converts a multiobjective optimization problem into the equivalent single-objective optimization problem by introducing an aspiration level that corresponds to the user's preference for each objective function value. As shown in Fig. 5, the Pareto optimal solution is usually located on the line connecting the ideal point and the aspiration level in the objective function space, regardless of whether or not the aspiration level lies in the feasible region. STOM is formulated as the following min-max problem:

$$\text{Minimize : } \max_{i=1,2,\dots,r} w_i(f_i(\mathbf{x}) - f_i^I) \quad (14)$$

$$\text{subject to : } g_j(\mathbf{x}) \geq 0 \quad (j = 1, 2, \dots, m)$$

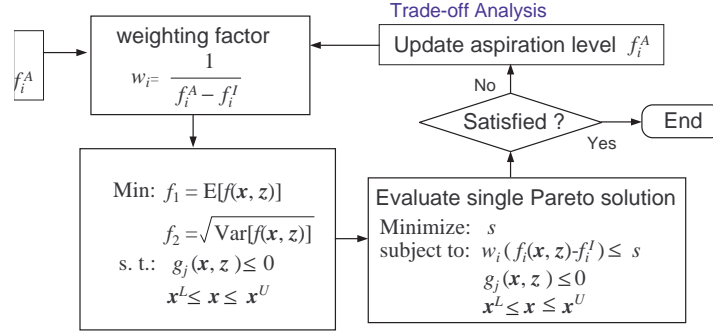


Figure 6. Flowchart of robust multiobjective optimization using STOM

where f_i^I is an ideal point and w_i is a weight coefficient that is evaluated by using an aspiration level f_i^A as follows:

$$w_i = \frac{1}{f_i^A - f_i^I} \quad (i = 1, \dots, r)$$

Introducing a slack variable s , the equivalent single-objective optimization problem is defined:

$$\begin{aligned} \text{Minimize: } & s & (15) \\ \text{subject to: } & w_i (f_i(\mathbf{x}, \mathbf{z}) - f_i^I) \leq s \quad (i = 1, \dots, r) \\ & g_j(\mathbf{x}, \mathbf{z}) \leq 0 \quad (j = 1, \dots, m) \end{aligned}$$

The Pareto solution corresponding to the aspiration level is obtained. When the user is not satisfied with the obtained solution, the user repeats the process by changing the aspiration level. On the other hand, the Pareto surface can be obtained by parametrically changing the aspiration level.

The flow of the robust multiobjective optimization is illustrated in Fig. ???. In this study, the sequential quadratic method (SQP) is adopted to solve the equivalent optimization problem (15).

5 NUMERICAL EXAMPLES

The airfoil adopted in this study is Fx63-137 (maximum wing thickness 13.7%, maximum camber 5.97%) that motor gliders widely adopt, where the Reynolds number is set as $Re = 7.94 \times 10^5$ [3]. Here, the lift maximization design under the case of 10 degree of the morphing angle is illustrated.

The design variables are the y coordinates of the NURBS passing points y_3 for P_3^u and y_4 for P_4^u and the angle of attack for the nominal airfoil α' . Note that α' is different from the angle of attack for the morphed airfoil. In order to avoid the ill-shaped airfoil that has ill effects on the accuracy of the surrogate model, the design variables for 10 degree of the morphing angle are constrained as follows:

$$0.06355 \leq y_3 \leq 0.11855 \quad (16)$$

$$-0.07165 \leq y_4 \leq 0.02835 \quad (17)$$

$$-6.0 \leq \alpha' \leq 5.0 \quad (18)$$

Note that the lower and upper bounds are varied for the morphing angle. In addition, the angle of attack α' is also constrained to avoid numerical errors beyond the stall angle for the aerodynamic analysis.

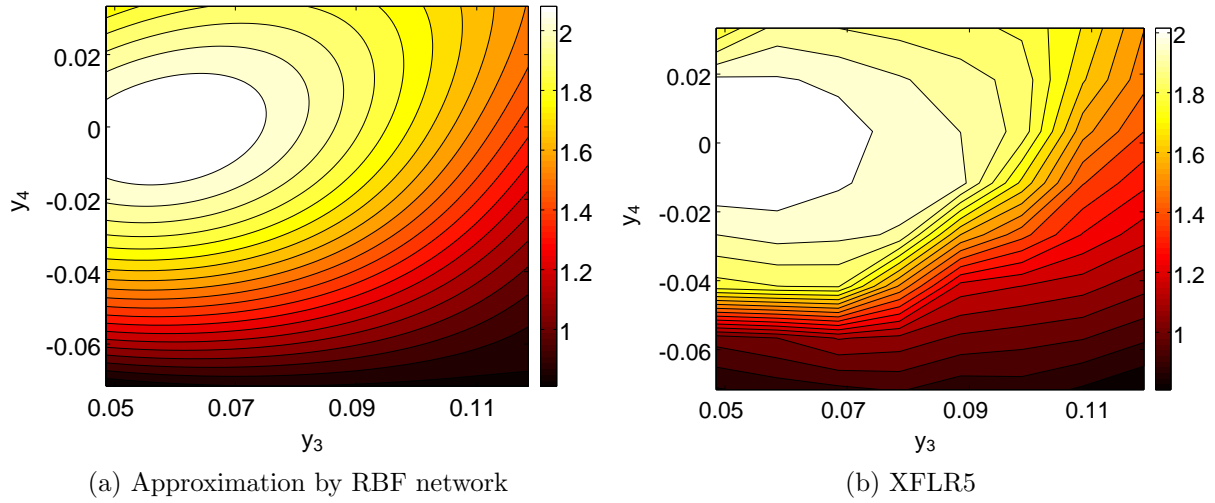


Figure 7. C_L distribution for $\alpha' = 2^\circ$ in design variable space

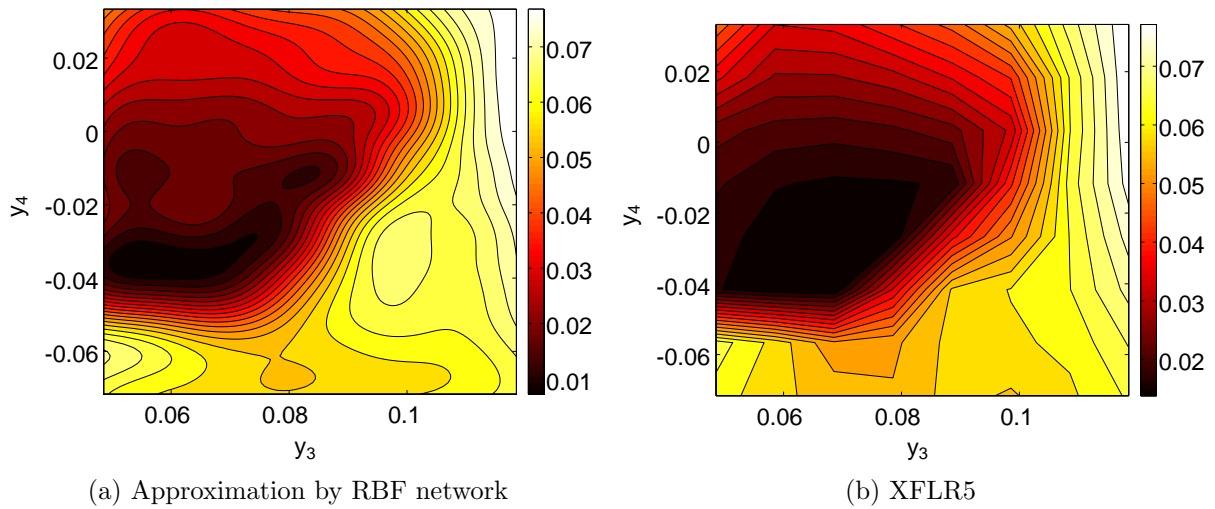


Figure 8. C_D distribution for $\alpha' = 2^\circ$ in design variable space

5.1 Approximation Accuracy of RBF Network

The approximation accuracy of the RBF network is compared for the airfoil under the case of 10 degree of the morphing angle. The lift and the drag coefficient distribution in terms of the design variables y_3 and y_4 for the angle of attack to the nominal airfoil $\alpha' = 2^\circ$ are illustrated in Figs. 7 and 8, respectively. In the figures, (a) indicated the approximated contour curve evaluated by the RBF network, and (b) is a contour plot made from the XFLR5 results at the lattice points. Because of the lattice points is small in number, the contour curves in (b) are shaky. It is found from the figures that the RBF network has sufficient approximation accuracy for the lift coefficient. However, the accuracy for the drag coefficient is insufficient, though the overall trends are very similar from each other. This is because the change of the drag coefficient is much larger for the stall regions in comparison of that of the lift coefficient.

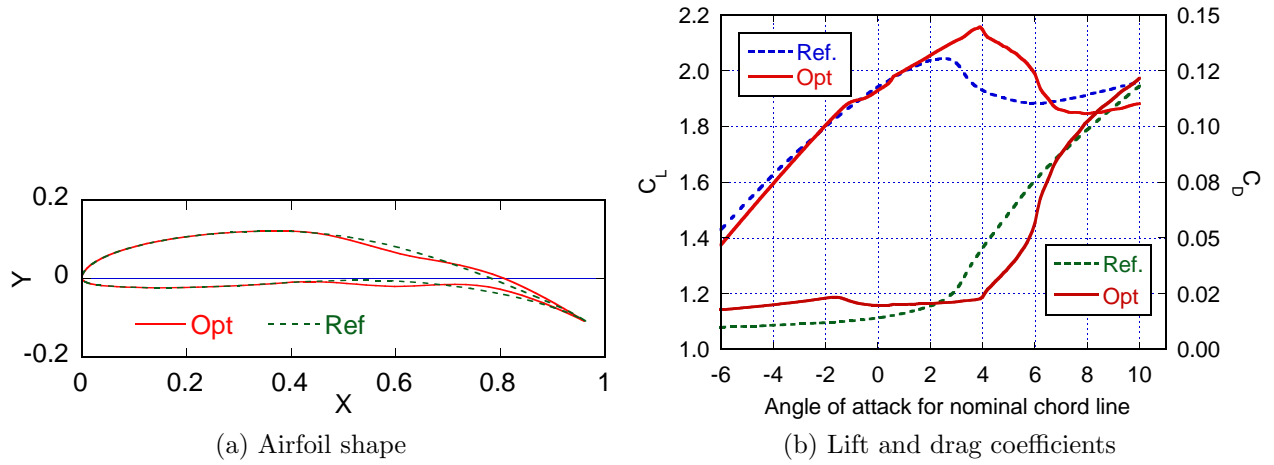


Figure 9. Comparison of C_{Lt} maximized airfoil shape and the referred airfoil [3] for 10 degree of morphing angle

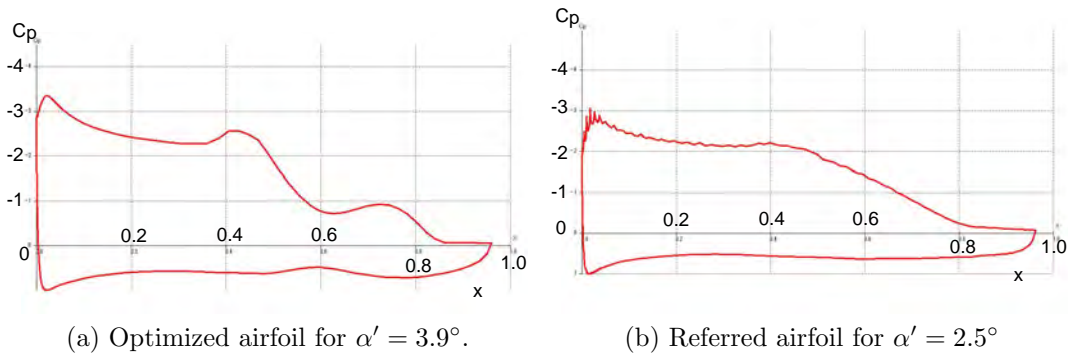


Figure 10. Comparison of pressure distributions at the maximum lift coefficient

5.2 Lift Coefficient Maximization as Deterministic Design

The lift coefficient maximization design for 10 degree of the morphing angle is illustrated in Fig. 9(a). In this figure, “Opt” curve corresponds to the optimized design and “Ref” to the airfoil shape in the reference [3]. Though the optimized airfoil has wavy shape, the maximum lift coefficient is larger than that of the reference airfoil as illustrated in Fig. 9(b), where the horizontal axis indicates the angle of attack for the nominal airfoil (α').

The maximum lift coefficient of the optimum airfoil is 2.157 at $\alpha' = 3.9^\circ$. It is better than that of the referred airfoil, 2.0443 at $\alpha' = 2.5^\circ$. On the other hand, the drag coefficient is about twice as that of the referred wing because of the wavy shape. However, the optimum airfoil has smaller drag coefficient at the stall angle. The pressure distribution is compared in Fig. 10. The horizontal axis indicates the chord line of the nominal airfoil and the lateral axis indicates the pressure coefficient, where the negative value is the upper side. That is, upper curve corresponds to the upper airfoil side. In the optimized airfoil, the negative pressure decreases at the wavy point, but the value is recovered at the backward. That’s why the optimum airfoil has larger lift coefficient.

The approximation accuracy is shown in Table 1, where the approximated and the analyzed values

Table 1. Approximation accuracy at the optimum design

Design	Method	$C_{L_{max}}$	α' (deg)
Optimum	RBFN	2.158	3.09
	XFLR5	2.157	3.90
Reference [3]	XFLR5	2.044	2.50

are compared for the optimized and the referred airfoil. Though the difference of the maximum lift coefficient is small, the stall angle has large difference. It indicated that some improvements are required to establish the approximation accuracy.

5.3 Robust Multiobjective Optimization

Here illustrates the Pareto solutions for the robust multiobjective optimization problem to maximize the lift coefficient, while to minimize the variation of the lift coefficient with respect to the airfoil shape. Considering variations of the airfoil shape, y_3 and y_4 are set as random variables and the standard deviations are set as follows:

$$\sqrt{\text{Var}[y_i]} = 0.01 \quad (i = 3, 4) \quad (19)$$

The design variables are set as the mean values of the coordinates, $E[y_3]$, $E[y_4]$ and the angle of attack for the nominal airfoil, α' . The design problem is formulated as the robust multiobjective optimization problem as follows:

$$\begin{aligned} \text{Maximize: } & f_1 = C_L(E[y_3], E[y_4], \alpha') \\ \text{Minimize: } & f_2 = \sqrt{\text{Var}[C_L(E[y_3], E[y_4], \alpha')]} \\ & y_i^L \leq E[y_i] \leq y_i^U \quad (i = 3, 4) \\ & \alpha'_L \leq \alpha' \leq \alpha' \end{aligned} \quad (20)$$

where the same side constraints as the deterministic design problem are used.

Pareto solutions obtained by parametrically changing the aspiration levels are illustrated in Fig. 11(a). The ideal point is located at the lower right corner, because f_1 (mean value of C_L) will be maximized and f_2 (standard deviation of C_L) will be minimized, where the ideal point is set for both solutions for the single objective optimizations. It is found that the obtained Pareto solutions are located on the line connecting the ideal point and the aspiration levels.

The mean airfoil shapes corresponding to A, B and C denoted in Fig. 11(a) are compared in Fig. 11(b). The solution C that has large mean value of C_L and large variance of C_L is a wavy shape as the deterministic design shown in Fig. 9. On the other hand, the smaller variance designs like B and A have smaller wavy shape. Therefore, the STOM obtains reasonable Pareto solutions.

Finally, the approximation accuracy of the surrogate model is presented. Table 2 compares the approximated C_L by the RBF network with the numerical value by XFLR5 for the obtained airfoil shapes, A, B and C. It is found that the approximation has the sufficient accuracy as the previous examples.

6 CONCLUSIONS

This study evaluates the robust optimum airfoil shape of the morphing wing by the robust multiobjective optimization method by using STOM. Through numerical examples, the following conclusions are remarked.

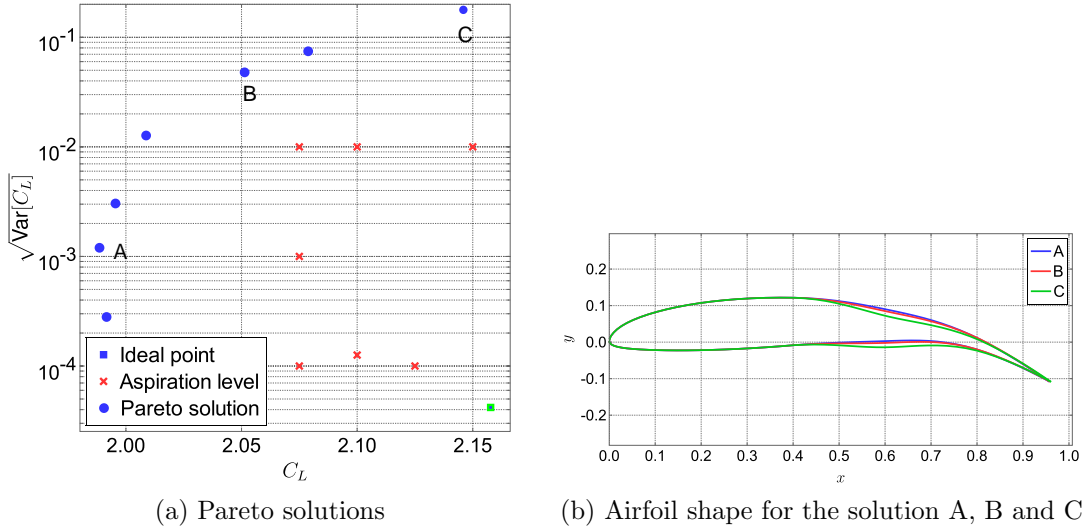


Figure 11. Pareto solutions for robust multiobjective optimization

Table 2 Approximation accuracy by RBF network for the Pareto solutions A, B and C in Fig. 11(a)

Pareto solution	RBF network		XFLR5	
	$E[C_{L_{max}}]$	α' (deg)	$E[C_{L_{max}}]$	α' (deg)
A	1.989	3.48	2.007	3.30
B	2.051	3.71	2.056	3.70
C	2.146	3.30	2.132	3.90

- The morphing section is modeled by using the NURBS curve in order to reduce the number of design variables, where the passing points of the NURBS curve are treated as design variables. The smooth connection of the leading edge side and the morphing section at the trailing edge side at the morphing starting point is established by setting the double starting points of the NURBS curve at the morphing beginning points.
- The aerodynamic performance is evaluated by using the analysis tool XFLR5 for low Reynolds number region. To avoid the direct calls of the analysis tool during the optimization, the surrogate model is constructed by using the RBF network. Through numerical examples, the approximation accuracy of the lift coefficient is demonstrated to be sufficient, though some improvements will be required for the drag coefficient approximation.
- The robust multiobjective optimization considering variation of the airfoil shape is demonstrated, where the mean value and the standard deviation of the lift coefficient are formulated as individual objective functions. The Pareto solution obtained by STOM is illustrated to be effective to visualize the trade-off between the mean value and the standard deviation.

The other performance index such as the lift-to-drag ratio should be considered. Then, design methodology for the corrugation arrangement corresponding to the optimized airfoil shape should be established in the future that requires the multidisciplinary coupling analysis with aerodynamics and structure.

REFERENCES

1. Tamayama, M., "Survey on Morphing Activities", *Journal of Japan Society of Fluid Mechanics*, Vol. 28, No. 4, 2009, pp. 277-284, (in Japanese)
2. Barbarino, S., Bilgen, O., Ajaj, R. M., Friswell, M. I., and Inman, D. J., "A Review of Morphing Aircraft", *Journal of Intelligent Material Systems and Structures*, Vol. 22, No. 9, 2011, pp. 823-877.
3. Yokozeki, T., Sugiura, A., and Hirano, Y., "Development of Variable Camber Morphing Airfoil Using Corrugated Structure", *Journal of Aircraft*, Vol. 51, 2014, pp. 1023-1029.
4. Yokozeki, T., Takahashi, H., and Hirano, Y., "Development and Demonstration of Morphing Wing Using Corrugated Structures", *Proceedings of 46th JSASS Annual Meeting*, 2015, JSASS-2015-1008, pp. 1-5, (in Japanese)
5. Toyoda, M., and Kogiso, N., "Robust Multiobjective Optimization Using Satisficing Trade-Off Method", *Journal of Mechanical Science and Technology*, Vol. 29, 2015, pp. 1361-1367.
6. Nakayama, H. and Sawaragi, Y., "Satisficing Trade-Off Method for Multiobjective Programming", *Lecture Notes in Economics and Mathematical Systems*, Vol. 229, 1984, pp. 113-122.
7. Kodama, R., Kogiso, N., Toyoda, M., and Tanaka, H., "Trade-Off analysis for Structural Design of High-Precision Space Reflector Using Multiobjective Optimization Method", *Mechanical Engineering Journal*, Vol. 2, No. 4, 2015, 15-00058, pp. 1-14.
8. Pieggl, L., and Tiller, W., *The NURBS Book*, 2nd ed., Springer, 1997.
9. Oyama, A., and Fujii, K., "A Study on Airfoil Design for Future Mars Airplane", *44th AIAA Aerospace Sciences Meeting*, 2006, AIAA-2006-1484.
10. Kogiso, N., Hirajo, D., and Akita, T., "Shape Optimal Design of Membrane Wrinkling Minimization Using NURBS Curves", *Journal of the Japan Society for Aeronautical and Space Sciences*, Vol. 56, 2008, pp. 72-79, (in Japanese)
11. "XFLR5, An Analysis Tool for Airfoils, Wings and Planes", <http://www.xflr5.com/xflr5.htm>, (access on 2015. 10)
12. Forrester, A., Sobester, A., and Keane, A., *Engineering Design Via Surrogate Modeling: A Practical Guide*, Wiley, 2008.
13. Orr, M. J. L., *Introduction to Radial Basis Function Networks*, University of Edinburgh, <http://www.anc.ed.ac.uk/rbf/rbf.html>, 1996, pp. 1-67, (access on 2015. 10).
14. Kitayama, S., Arakawa, M. and Yamazaki, K., "Sequential Approximate Optimization Using Radial Basis Function Network for Engineering Optimization", *Optimization and Engineering*, Vol. 12, No. 4, 2011, pp. 535-557.